Probing the $_{31}$Ga ground-state properties in the region near $Z = 28$ with high-resolution laser spectroscopy

G. J. Farooq-Smith,[1,2,*] A. R. Vernon,[2] J. Billowes,[2] C. L. Binnersley,[2] M. L. Bissell,[2] T. E. Cocolios,[1,2] T. Day Goodacre,[2,3,†] R. P. de Groote,[1] K. T. Flanagan,[2] S. Franchoo,[4] R. F. Garcia Ruiz,[1,2] W. Gins,[1] K. M. Lynch,[5] B. A. Marsh,[3] G. Neyens,[1] S. Rothe,[2,3] H. H. Stroke,[6] S. G. Wilkins,[2] and X. F. Yang[1]

[1]*KU Leuven, Instituut voor Kern- en Stralingsfysica, Celestijnenlaan 200D, 3001 Leuven, Belgium*
[2]*School of Physics and Astronomy, The University of Manchester, Manchester M13 9PL, United Kingdom*
[3]*EN Department, CERN, CH-1211 Geneva 23, Switzerland*
[4]*Institut de Physique Nucléaire d'Orsay, F-91406 Orsay, France*
[5]*ISOLDE, EP Department, CERN, CH-1211 Geneva 23, Switzerland*
[6]*Department of Physics, New York University, New York, New York 10003, USA*

(Received 7 July 2017; revised manuscript received 15 September 2017; published 23 October 2017)

Magnetic-dipole and electric-quadrupole moments for $^{65,67,69,75,79-82}$Ga are reported using the Collinear Resonance Ionization Spectroscopy (CRIS) technique at the ISOLDE facility, CERN. The moments of ^{65}Ga have been measured for the first time: $\mu = +1.775(3)\ \mu_N$ and $Q_s = +21.0(15)\ e\,\mathrm{fm}^2$. These results are compared to shell-model calculations using the GXPF1 and JUN45 interactions and the trends of the moments approaching the region of the doubly magic ^{56}Ni are discussed. Additionally, new values for the change in mean-square charge radii for ^{65}Ga and ^{67}Ga allow investigation into the odd-even staggering in the region below $N = 40$.

DOI: 10.1103/PhysRevC.96.044324

I. INTRODUCTION

Over the past few decades, the investigation of the ground-state properties of isotopes residing in the vicinity of the shell closure $Z = 28$ has attracted significant interest. In the region near the doubly magic isotope $^{78}_{28}$Ni$_{50}$, there are signatures of shape coexistence: low-energy intruder states in the nearby $N = 49$ isotones [1,2] and the observation of an intruder 0^+_2 state in ^{80}Ge [3]. A kink at $N = 50$ in the relative mean-square charge radii for the gallium isotopes adds further confirmation to its status as a magic number [4,5], and several theoretical studies have been dedicated to the study of this magic number [6–9].

Additionally, the reversal of the $\pi 1f_{5/2}$ and $\pi 2p_{3/2}$ orbitals can be attributed to an attractive monopole interaction which strengthens as the neutron $\nu g_{9/2}$ orbital gets filled [10]. This eventually manifests itself with a ground-state spin change and has been observed for the copper and gallium isotope chains: in ^{75}Cu [11] and ^{79}Ga [12] respectively. The monopole tensor interaction has also been important for explaining the triple shape coexistence exhibited in ^{70}Ni [13], along with the presence of proton and neutron excitations across the $Z = 28$ shell gap. The inclusion of these cross-shell excitations in shell-model calculations has recently helped explain the systematics of the nuclear electromagnetic moments for this region, such as the electric quadrupole moments in the manganese isotopes [14]. However, the amount of excitations required in shell model calculations to explain evolutions in shell gaps and single-particle energies still remains to be discovered.

For the neutron-deficient region above $Z = 28$, a sudden increase in the magnetic moment was observed for ^{57}Cu, towards the effective single-particle $\mu(\pi p_{3/2})$ value [15]. While $N, Z = 28$ are still good magic numbers in this region of the nuclear chart, a softer $^{56}_{28}$Ni$_{28}$ was required to obtain good agreement between experiment and theoretical predictions [16]. However, the electric-quadrupole moments are a better probe of the softness of the core, due to the strong correlation of collectivity with pair scattering across the orbitals. Later studies of the copper quadrupole moments revealed an increasing collectivity as $N = 28$ is approached and reinforced the suggestion of a soft core [17], although they could not reach $N < 29$. Similar studies into these moments for the neutron-deficient gallium isotopes will provide additional insight into this phenomenon.

In this article, we report on the measurements of the radioactive gallium isotopes $^{65,67,69,75,79-82}$Ga. Newly presented magnetic dipole and electric quadrupole moments for ^{65}Ga are compared to shell-model calculations from recent interactions, helping to characterize the systematics in the neutron-deficient region below $N = 40$. Changes in the mean-square charge radii for ^{65,67}Ga are also presented alongside literature values for other gallium isotopes. Where available, data are compared to literature values, showing good agreement and a similar precision for the moments and changes in the mean-square charge radii.

II. EXPERIMENTAL METHOD

Beams of radioactive gallium isotopes were produced at the ISOLDE facility in CERN [18] by first impinging 1.4 GeV

*gregoryjames.farooqsmith@kuleuven.be
†Present address: TRIUMF, Vancouver, British Colombia V6T 2A3, Canada.

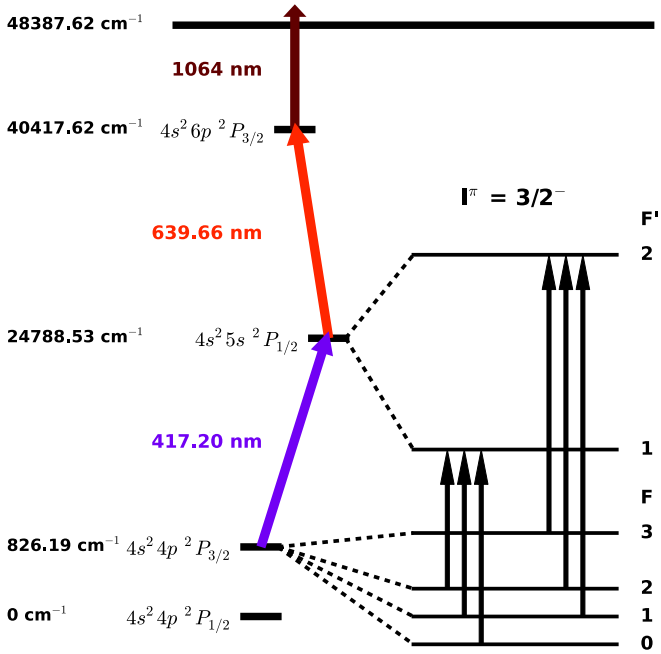

FIG. 1. A diagram of the resonance ionization scheme used for neutral gallium, including the allowed hyperfine transitions (not to scale) for the 417.2-nm transition, assuming $I^\pi = 3/2^-$.

protons from the Proton-Synchrotron Booster [19] onto a solid tungsten neutron converter [20]. Neutrons produced from the resulting spallation processes irradiated a thick UC_x target to induce fission events. From this, gallium isotopes diffused out of the target material and effused towards a high temperature ($\sim$ 2200 K) tantalum ion source, where they were laser-ionized using the Resonance Ionization Laser Ion Source (RILIS) [21], and extracted at 30 keV. The mass regions of interest were selected using the high-resolution mass separator [18] and subsequently cooled and bunched using the ISOLDE cooler buncher (ISCOOL) [22,23].

After reaccelerating to 30 keV, the ion bunches were electrostatically deflected into the collinear resonance ionization spectroscopy (CRIS) beamline [26–28] and passed through a Charge Exchange Cell (CEC). This was filled with a potassium vapor (held at 460–470 K), which neutralized the ion bunches with a neutralization efficiency of 2.5%. At this temperature, charge-exchange calculations based on the work of Rapp and Francis [29] showed that the ground and metastable states (as shown in Fig. 1) are roughly equally populated. Any non-neutralized components remaining were deflected away. After passing through a differential-pumping region (just after the CEC), the neutralized atomic bunches entered the laser-atom interaction region. They were collinearly overlapped with the laser pulses and synchronized with the duty cycle of the laser system. The ionization scheme used in the experiment is shown in Fig. 1 and probes the same transition from previous work on gallium isotopes [2,12,24]. 417.2-nm laser light was produced by frequency-doubling light from an M-Squared SolsTiS continuous-wave Ti:Sa laser (pumped by a Sprout G-18 18W continuous-wave DPSS laser), using an ECD-X frequency doubler. The chopping of this light was performed with the Pockels cell setup as detailed in Ref. [30]. A 35-m multimode optical fibre was used to transport the 417.2-nm laser light from the CRIS laser laboratory to the CRIS beamline. The 639.7-nm light was produced from a Spectron pulsed dye laser, pumped with 532-nm light from a Litron LPY-601 Nd:YAG laser. This laser system had two laser heads which could be controlled independently. The other laser head produced the 1064-nm light required for the ionization step. The interaction region was maintained at 2×10^{-8} mbar to minimize the background due to nonresonant collisional ionization with gas molecules and isobaric contamination (such as rubidium). After resonant excitation and laser ionization, the ions were detected by deflecting them onto a Hamamatsu F4655-12 positive-ion microchannel plate (MCP) detector biased at -2250 V.

III. ANALYSIS AND RESULTS

Previous use of the target-ion-source unit with direct impact of the protons on the target resulted in large beams of isobaric rubidium and strontium contamination. Produced via proton-induced fragmentation, long-lived and stable isotopes of these elements had accumulated in the target matrix and were released and surface ionized throughout the experiment. This prevented measurements of exotic gallium isotopes past ^{82}Ga from being performed. Despite relatively high count rates of ^{65,67}Ga in Fig. 2, considerable background rates are

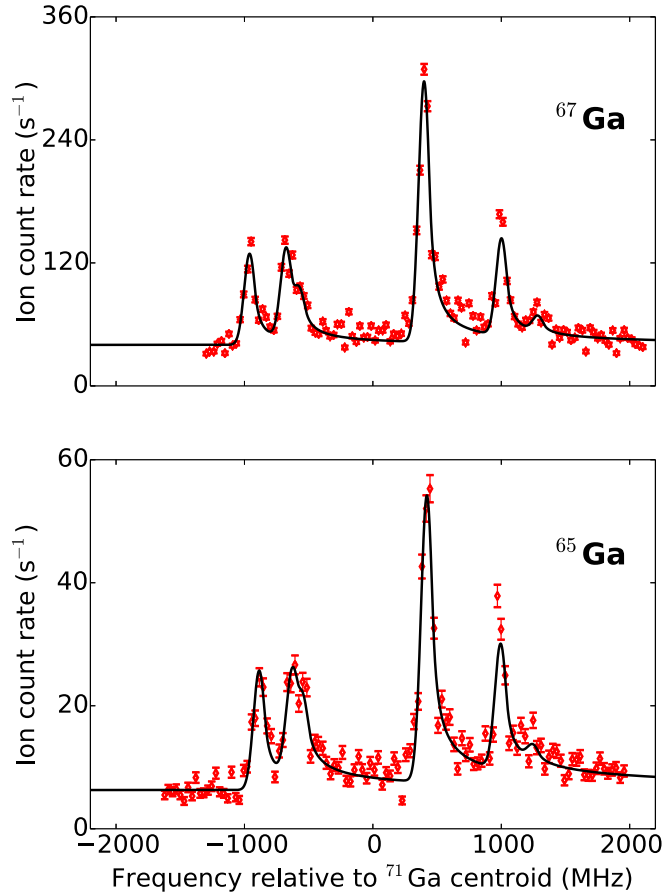

FIG. 2. Example hyperfine spectra for ^{65,67}Ga, using the $4p\ ^2P_{3/2} \rightarrow 5s\ ^2S_{1/2}$ transition. The solid lines are the best fit using an asymmetric Gaussian profile, assuming a spin assignment of $I = 3/2^-$.

TABLE I. The $A(4p\,^2P_{3/2})$ and $A(5s\,^2S_{1/2})$ factors and magnetic-dipole moments for the gallium isotopes studied in this experiment. Statistical uncertainties are enclosed with parentheses.

		$A(4p\,^2P_{3/2})$ (MHz)		$A(5s\,^2S_{1/2})$ (MHz)		μ (μ_N)		
A	I	This work	Cheal *et al.*[a]	This work	Cheal *et al.*[a]	This work	Cheal *et al.*[a]	Ref. [25]
65	3/2	+166.7(6)		+940.3(13)		+1.774(3)		
67	3/2	+174.7(38)	+175.8(10)	+978.0(61)	+979.7(25)	+1.845(12)	+1.848(5)	+1.8507(3)
69	3/2	+189.8(13)	+191.5(9)	+1067.7(18)	+1069.5(15)	+2.014(4)	+2.018(4)	+2.01659(5)
71	3/2	+242.7(6)	+242.8(7)	+1357.7(17)	+1358.2(16)			+2.56227(2)
75	3/2	+172.6(1)	+173.6(9)	+971.7(12)	+973.1(15)	+1.833(3)	+1.836(4)	
79	3/2	+97.3(38)	+98.3(9)	+550.2(112)	+555.0(14)	+1.038(21)	+1.047(3)	
80g	6[b]	+1.4(7)[c]	+0.9(1)[c]			+0.061(29)[d]	+0.036(4)[d]	
80m	3[b]	−68.0(2)[c]	−67.5(1)[c]			−1.435(5)[d]	−1.425(5)[d]	
81	5/2	+98.6(10)	+98.9(4)	+555.7(26)	+555.6(13)	+1.747(8)	+1.747(5)	
82	2[b]			+178.7(49)[c]	+182.5(14)[c]	+0.449(12)	+0.459(4)	

[a]Values taken from Refs. [2,12,24].
[b]Spins based on suggested assignments for ^{80}Ga [2] and ^{82}Ga [24].
[c]$A(5s\,^2S_{1/2})/A(4p\,^2P_{3/2})$ constrained to +5.592(9) [12].
[d]Magnetic moment calculated using $A(4p\,^2P_{3/2})$ values.

also observed. This contamination is suspected to be stable titanium compounds [31] and has already been reported in previous studies around the same mass region at the ISOLDE facility [32].

The extraction of the ground-state properties from the hyperfine spectra for each isotope was performed with a χ^2-minimization routine [33]. High-frequency tails have been observed in all spectra analysed in this experiment, resulting from AC Stark shift effects induced by the high power of the ionization laser. Although recent studies have suggested these distortions can be removed by delaying the ionization laser light [34], the short lifetime of the $5s\,^2S_{1/2}$ state ($t_{1/2}$ = 5.7(6) ns [35]) did not permit this. Therefore, asymmetric fitting profiles defined by a Gaussian function with a power-law high-frequency tail were used (colloquially referred to as the Crystal Ball function) [36,37]. The analysis of the data was performed with no restrictions on the A and B hyperfine parameters and the intensities of the hyperfine peaks, apart from the case of ^{80g,m}Ga.

Spin assignments were deduced by comparing ratios of the resulting A-hyperfine factors for a particular spin assignment to $A(5s\,^2S_{1/2})/A(4p\,^2P_{3/2}) = +5.592(9)$, arising from the weighted mean of ratios for gallium isotopes measured in Ref. [12]. Magnetic-dipole and electric-quadrupole moments were extracted from the known ratios $\mu = \mu_{\rm ref} I A / I_{\rm ref} A_{\rm ref}$ and $Q_s = B Q_{\rm ref}/B_{\rm ref}$ and are displayed in Tables I and II, respectively. Measured observables were determined relative to ^{71}Ga, using $A_{\rm ref}(5s\,^2S_{1/2}) = +1358.2(16)$ MHz [12], $\mu_{\rm ref} = +2.56227(2)\,\mu_N$ [25], $B_{\rm ref}(4p\,^2P_{3/2}) = +39(2)$ MHz [12], and $Q_{\rm ref} = +10.7(1)\,e\,{\rm fm}^2$ [39]. The low Z of gallium meant that sensitivity to the hyperfine anomaly could be neglected [40].

Isotope shifts were extracted by comparing the centroid frequency of a given spectrum to the nearest ^{71}Ga spectrum taken in time. These values are presented in the second column of Table III and compared with values from previous studies in the fourth column [4]. Additionally, Fig. 3 plots these values from both studies against each other. The systematic offset

TABLE II. The $B(4p\,^2P_{3/2})$ factors and electric-quadrupole moments for the gallium isotopes studied in this experiment. Statistical uncertainties are enclosed with parentheses.

		$B(4p\,^2P_{3/2})$ (MHz)		Q_s ($e\,{\rm fm}^2$)		
A	I	This work	Cheal *et al.*[a]	This work	Cheal *et al.*[a]	Refs. [38,39]
65	3/2	+75(1)		+20.7(11)		
67	3/2	+71(4)	+73(4)	+19.5(15)	+19.8(16)	+19.7(2)
69	3/2	+61(8)	+63(2)	+16.7(24)	+17.1(11)	+17.1(2)
71	3/2	+38(3)	+39(2)			+10.7(1)
75	3/2	−107(2)	−105(1)	−29.5(16)	−28.5(17)	
79	3/2	+49(12)	+58(2)	+13.4(33)	+15.8(10)	
80g	6[b]	+186(7)	+174(3)	+50.7(35)	+47.8(27)	
80m	3[b]	+132(3)	+137(3)	+35.8(23)	+37.5(21)	
81	5/2	−12(5)	−18(3)	−3.3(13)	−4.8(8)	
82	2[b]	+74(29)	+72(3)	+20.0(80)	+19.7(13)	

[a]Values taken from Refs. [2,12,24].
[b]Spins based on suggested assignments for ^{80}Ga [2] and ^{82}Ga [24].

TABLE III. Isotope-shift values for the isotopes studied in this work. Statistical and systematic uncertainties are enclosed in parentheses and square brackets respectively. See text and Fig. 3 for further details.

	$\delta\nu^{71,A}$ (MHz)		
A	This work	Corrected values	Procter *et al.* [4]
65	+101(5)	+106(6)[0.8]	
67	+74(11)	+77(12)[0.6]	
69	+33(35)	+34(36)[0.3]	+40(4)
71	0	0	0
75	−44(4)	−46(4)[0.4]	−45(2)
79	−173(11)	−182(12)[1.4]	−186(2)
80g	−230(4)	−241(4)[1.8]	−239(4)
80m	−224(4)	−235(5)[1.8]	−232(3)
81	−252(7)	−264(8)[2.0]	−272(2)
82	−207(4)	−217(5)[1.7]	−222(9)

between the two data sets is highlighted by the deviation of the green dotted and blue solid lines. It can be attributed to an offset in the ISCOOL acceleration voltage, which is known to vary between experiments at the ISOLDE facility [4,41,42]. In order to directly compare between the two data sets, isotope shifts

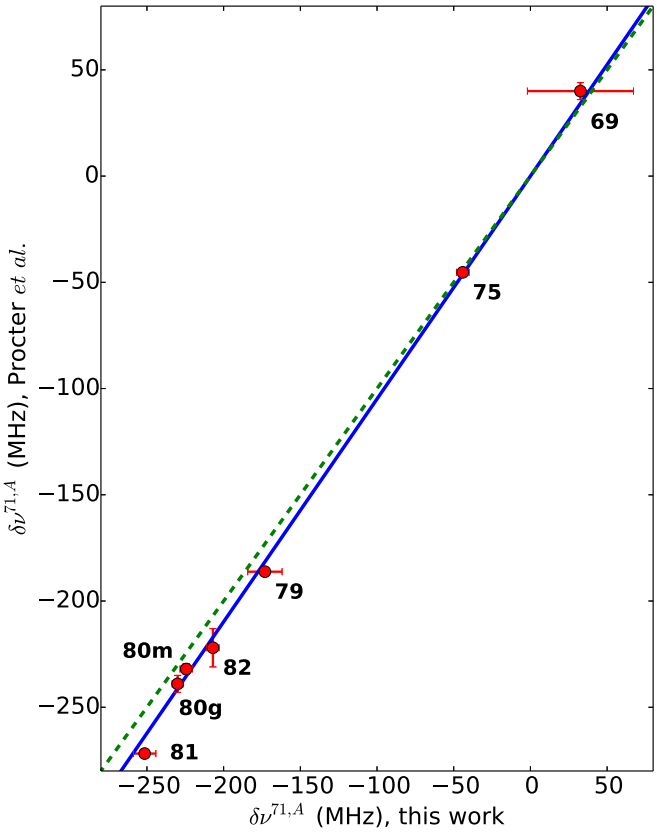

FIG. 3. Isotope shift values from literature [4] plotted against this work. The green-dotted line represents consistency between the two data sets and the blue solid line represents the current relation between the two. Each data point is labeled according to the mass number involved.

obtained in this study were modified by applying a correction factor given by the gradient difference between the two lines in Fig. 3, given by

$$\delta\nu^{71,A}_{\mathrm{Mod}} = 1.049(8)\delta\nu^{71,A}_{\mathrm{CRIS}}, \tag{1}$$

where $\delta\nu^{71,A}_{\mathrm{Mod}}$ represents modified isotope shifts obtained in this study, which are presented in the third column of Table III. This modification benchmarks these values to previous literature [4] and, in particular for ^{65,67}Ga, makes them directly comparable to the rest of the isotope shifts that have already been obtained across the gallium chain. The associated error represents an additional systematic uncertainty and is quoted separately for the modified isotope shifts given in Table III. Changes in the mean-square charge radii were calculated from the modified isotope shifts by using the equation

$$\delta\nu^{AA'} = M_{417}\frac{A'-A}{AA'} + F_{417}\delta\langle r^2\rangle^{AA'}, \tag{2}$$

where A and A' are the atomic masses assigned to the reference and measured isotopes respectively [45]. The parameters $M_{417} = -211.4(210)$ GHz amu and $F_{417} = 0.40(6)$ GHz/fm^2 represent the atomic factors and contain all the optical dependence for the 417.2-nm transition [4]. Reported hyperfine coefficients and isotope shift values for $^{67,69,75,79-82}$Ga in Tables I, II, and III are consistent with tabulated literature values [2,4,12,24]. Hyperfine parameters for $A(^2P_{3/2})$, $A(^2S_{1/2})$, $B(^2P_{3/2})$, and $\delta\nu^{71,A}_{\mathrm{CRIS}}$ were determined from a weighted mean of values obtained from the analysis of individual hyperfine spectra. Statistical uncertainties were determined from a weighted standard deviation of the individual values.

IV. DISCUSSION

A. Electromagnetic moments for $28 \leqslant N \leqslant 40$

An analysis of the hyperfine A factors for ^{65}Ga revealed ratios of +5.641(32) and +5.686(37) for $I = 3/2^-$ and $I = 5/2^-$ assignments. This results in standard deviations of 1σ and 2σ, respectively, from +5.592(9) [12]. Therefore, $I = 3/2^-$ is assigned for ^{65}Ga and confirms the ground-state spin

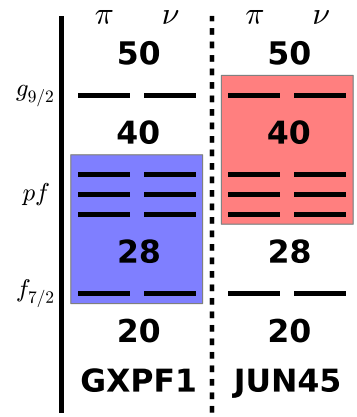

FIG. 4. A schematic representation of the model spaces involved for the GXPF1 and JUN45 interactions, shaded in blue and red respectively.

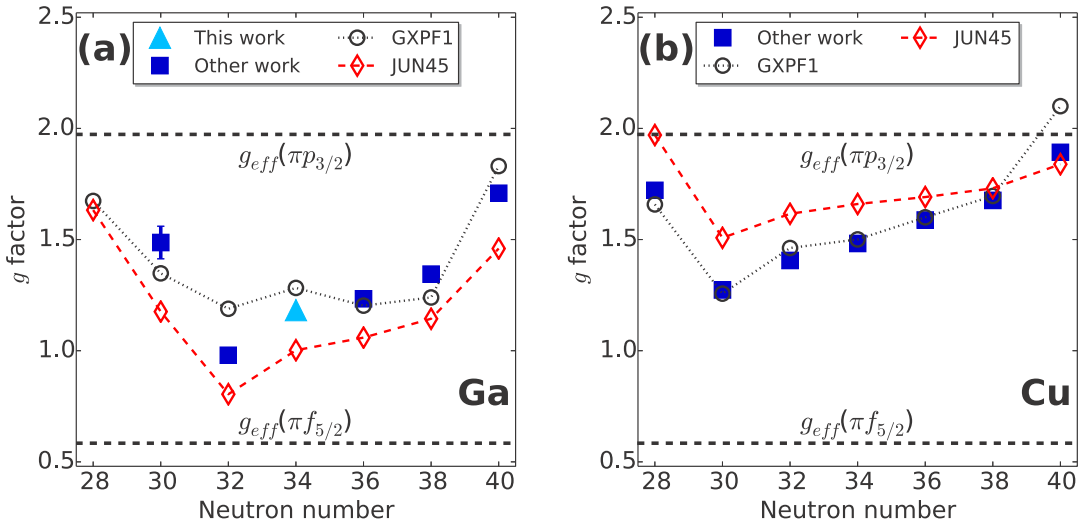

FIG. 5. (a) The extracted g factor for ^{65}Ga (light-blue triangle), alongside tabulated values across the gallium isotope chain from Refs. [4,25,43] (dark-blue squares). Apart from ^{61}Ga, the error bars are smaller than the marker size. (b) g factors for the odd-A copper isotopes in the same mass range [15] (dark-blue squares). Values are compared to GXPF1 (black circles) and JUN45 (red diamonds) calculations. Effective g-factor values for the $\pi p_{3/2}$ and $\pi f_{5/2}$ orbitals are illustrated with dashed lines.

assignment already made for this isotope [46]. Similar analyses for ^{67,69}Ga also confirm the ground-state spins of $I = 3/2^-$ as reported in Ref. [12].

Shell-model calculations of the nuclear moments for the lowest-lying $3/2^-$ states for $^{59-71}$Ga were performed using the KSHELL code [47] with two effective interactions: GXPF1 [48] and JUN45 [49]. The model spaces used for each interaction are displayed in Fig. 4. GXPF1 calculations are performed in a full pf model space with respect to the ^{40}Ca core. The values reported in this work are performed with up to 2p-2h excitations across the $N, Z = 28$ shell closures for the neutrons and protons, respectively. Calculations allowing up to 4p-4h excitations revealed that a convergence is reached at the 2p-2h level. This interaction has already been used to interpret the moments for the neutron-deficient odd-A copper isotopes down to ^{57}Cu [15,17], in addition to the quadrupole moments for the odd-A manganese isotopes in the same mass region [14].

The JUN45 calculations are performed starting from a ^{56}Ni core (see Fig. 4), including the upper pf orbits and the $g_{9/2}$ orbit as a valence space for both protons and neutrons. Calculations with this interaction were performed previously, in order to compare with moment measurements of ^{63,67,69,71}Ga [4,33]. In this article, we extend this study by including ^{59,61,65}Ga. The following effective g factors and effective charges were used for GXPF1: $g_s^{\rm eff} = 0.9 g_s^{\rm free}$, $g_l^{\rm eff} = +1.1, -0.1$ and $e_p^{\rm eff} = 1.5e$, $e_n^{\rm eff} = 0.5e$, respectively [48]. For JUN45, the values $g_s^{\rm eff} = 0.7 g_s^{\rm free}$, $g_l^{\rm eff} = +1.0, 0$ and $e_p^{\rm eff} = 1.5e$, $e_n^{\rm eff} = 1.1e$ were used [49].

The g factors for $^{61-71}$Ga are presented in Fig. 5(a). Values for the Cu isotope chain are presented alongside in Fig. 5(b) for comparison. With only one proton outside $Z = 28$, the GXPF1 calculations reproduce the Cu magnetic moments very well, due to the inclusion of excitations across the $N, Z = 28$ shell closures. Indeed with the JUN45 interaction, in which these excitations are not included in the model space, the Cu magnetic moment trends are less well reproduced. For the Ga isotopes however, the agreement of both GXPF1 and JUN45 interactions is similar.

Quadrupole moment values for the same isotopes are presented in Fig. 6. An increase towards the midshell at $N = 34$ (between $N = 28$ and the $N = 40$ subshell gap) confirms the increasing presence of neutron correlations, similar to the trend seen in the copper quadrupole moments [17]. Comparable parabolic trends can be seen in the experimental $B(E2)$ values between $N = 28$ and 50 for the nickel isotopes [50], and between $N = 50$ and 82 for the tin isotopes [51]. It is also

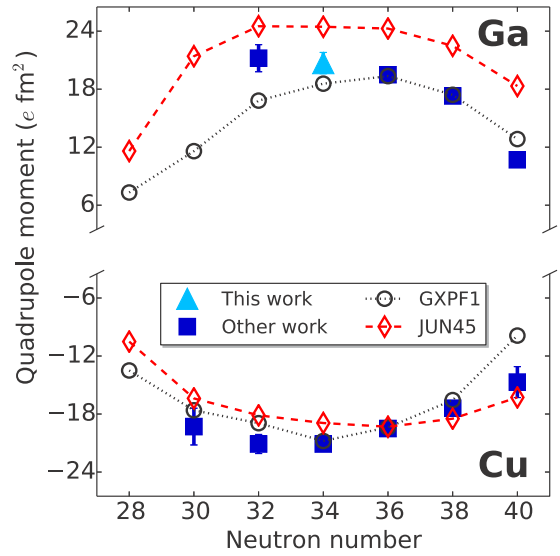

FIG. 6. The extracted electric quadrupole moment for ^{65}Ga (light-blue triangle), alongside literature values for the gallium [4,38] and copper [17,44] isotope chains (dark-blue squares). Values are compared to GXPF1 (black circles) and JUN45 (red diamonds) calculations.

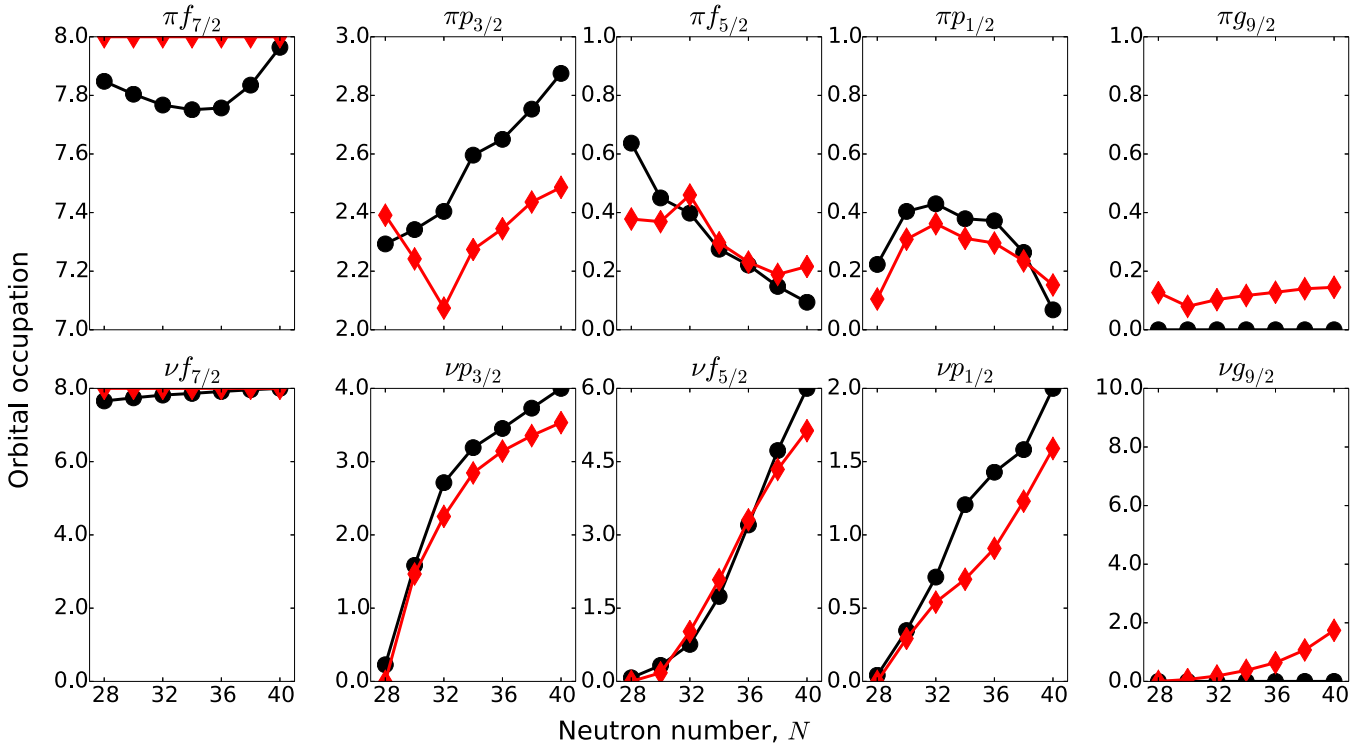

FIG. 7. Proton and neutron orbital occupations for odd-A $^{59-71}$Ga, across the combined orbital space for the GXPF1 (black circles) and JUN45 (red diamonds) interactions. Proton occupancies (top) are viewed with respect to the occupancy of a single proton, while neutron occupancies (bottom) are viewed with respect to the total occupancy for a given orbital.

noted that the quadrupole moments of the odd-A Ga isotopes and those of the odd-A Cu isotopes have a similar magnitude, but an opposite sign. This reflects the rather pure nature of these configurations: for a pure $\pi p^n_{3/2}$ configuration, one expects that $Q_{sp}(\pi p^1_{3/2},\text{Cu}) = -Q_{sp}(\pi p^3_{3/2},\text{Ga})$ [52].

Figure 7 illustrates the changes in the proton and neutron orbital occupations in the odd-A Ga wave functions, across the combined GXPF1 and JUN45 model spaces displayed in Fig. 4. The striking similarity between the trends in the JUN45 $\pi p_{3/2}$ orbital occupancies and the magnetic moment values described in Fig. 5 suggests that contributions from this orbital are important to describe the magnetic moments between $N = 28$ and 40. While the $^{59-71}$Ga moments predicted by JUN45 correspond to mixed $\pi p_{3/2}/\pi f_{5/2}$ configurations over the full range (due to the scattering of protons in the upper pf orbits), the $\pi p_{3/2}$ occupancy for GXPF1 increases towards $N = 40$. This illustrates how blocking the neutron orbits above $N = 40$ leads to reduced proton excitations across $Z = 28$ as the neutron shell is being filled. Furthermore, although proton and neutron excitations from the $f_{7/2}$ orbital are allowed in this case, this does not improve the reproduction of the experimental moment values.

B. Changes in the mean-square charge radii for ^{65,67}Ga

The changes in mean-square charge radii for ^{65,67}Ga are given in Table IV and displayed graphically alongside literature values in Fig. 8. For this discussion, neutron numbers are used for the charge-radii superscripts. Uncertainties quoted in Table IV originate from the statistical and systematic errors quoted in Table III, plus an additional systematic uncertainty from the F_{417} and M_{417} atomic factors. The odd-even staggering (OES) was investigated by calculating the $D(N;\delta\langle r^2\rangle^{40,N})$ parameter [53,54], given by

$$D(N;\delta\langle r^2\rangle^{40,N}) = (-1)^N\left[\delta\langle r^2\rangle^{40,N} - \frac{\delta\langle r^2\rangle^{40,(N-1)} + \delta\langle r^2\rangle^{40,(N+1)}}{2}\right], \quad (3)$$

and is also shown in Fig. 8. A normal odd-even staggering corresponds to positive D values, corresponding to odd-odd Ga isotopes having a slightly smaller charge radius than their odd-even neighbors. This is due to the odd neutron in even-N isotopes blocking the scattering of boson 0^+ pairs over several orbits from its own orbital [55].

Values with $D(N;\delta\langle r^2\rangle^{40,N}) < 0$ can be attributed to a reversal in OES. This has been observed in the $N \approx 40$ region not only with gallium [4], but also in the krypton and strontium

TABLE IV. Changes in the mean-square charge radii for ^{65,67}Ga ($N = 34,36$), using the modified experimental isotope shift values in Table III. The statistical, modified-systematic, and atomic-systematic uncertainties are enclosed within parentheses, square brackets, and curly brackets, respectively.

N	$\delta\langle r^2\rangle^{40,N}$ (fm^2)
34	−0.422(14)[2]{93}
36	−0.252(30)[2]{58}

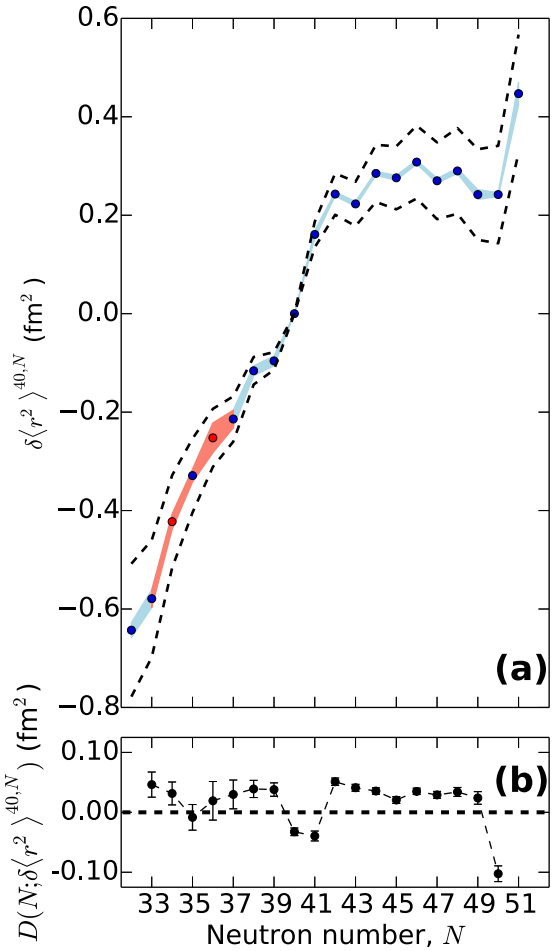

FIG. 8. (a) Changes in the mean-square charge radii across the gallium isotope chain. Red circles represent new measurements for ^{65,67}Ga ($N = 34,36$) and blue circles denote literature values [4]. Statistical and atomic systematic uncertainty bounds are given by the shaded areas and black-dotted lines respectively. (b) Corresponding $D(N;\delta\langle r^2\rangle^{40,N})$ values representing the odd-even staggering, calculated from Eq. (3).

chains [56]. It is also observed in the $N = 134$ region in the francium and radium chains, in which it coincides with a region of octupole deformation [54,57]. The reversal at $N = 50$ is caused by the dramatic increase in the charge-radius value of ^{82}Ga at $N = 51$, the signature of a shell closure crossing [4,5]. Further investigation with greater isotope shift sensitivity is also required to assert odd-even staggering characteristics at $N = 35$.

V. CONCLUSION

Gallium isotopes were studied at the CRIS experiment at ISOLDE, with the use of a three-step laser ionization scheme. The electromagnetic moments of ^{65}Ga and the changes in the mean-square charge radii for ^{65,67}Ga are reported. A comparison of the moments for $28 \leqslant N \leqslant 40$ with shell-model calculations suggest that, as protons occupy the upper pf orbits, calculations starting from a ^{56}Ni core reproduce the moments equally well as calculations that allow proton and neutron excitations across $N, Z = 28$. The inclusion of the $\nu g_{9/2}$ neutron orbit is only important for isotopes near $N = 40$. For the mean-square charge-radii values, an inverted odd-even staggering is observed around $N = 40$, although an explanation for this has not yet been proposed. A small inversion is observed also at $N = 35$; however, a remeasurement of the isotope shifts with better voltage precision is suggested to assert OES inversion in this region.

ACKNOWLEDGMENTS

We acknowledge the support of the ISOLDE Collaboration and technical teams. This work was supported by the ERC Consolidator Grant No. 648631; the IUAP-Belgian State Belgian Science Policy (BRIX network P7/12), FWO-Vlaanderen (Belgium) and GOA 15/010 from KU Leuven; the Science and Technology Facilities Council Consolidated Grant No. ST/F012071/1, Continuation Grant No. ST/J000159/1, and Ernest Rutherford Grant No. ST/L002868/1; and the European Union's Seventh Framework Programme for Research and Technological Development under Grant Agreements No. 262010 (ENSAR), No. 267194 (COFUND), and No. 289191 (LA^{3}NET). T.E.C. was supported by the STFC Ernest Rutherford Fellowship No. ST/J004189/1. We acknowledge the financial aid from the Ed Schneiderman Fund at New York University.

[1] X. F. Yang, C. Wraith, L. Xie, C. Babcock, J. Billowes, M. L. Bissell, K. Blaum, B. Cheal, K. T. Flanagan, R. F. Garcia Ruiz, W. Gins, C. Gorges, L. K. Grob, H. Heylen, S. Kaufmann, M. Kowalska, J. Kraemer, S. Malbrunot-Ettenauer, R. Neugart, G. Neyens, W. Nörtershäuser, J. Papuga, R. Sánchez, and D. T. Yordanov, Phys. Rev. Lett. **116**, 182502 (2016).

[2] B. Cheal, J. Billowes, M. L. Bissell, K. Blaum, F. C. Charlwood, K. T. Flanagan, D. H. Forest, S. Fritzsche, C. Geppert, A. Jokinen, M. Kowalska, A. Krieger, J. Krämer, E. Mané, I. D. Moore, R. Neugart, G. Neyens, W. Nörtershäuser, M. M. Rajabali, M. Schug, H. H. Stroke, P. Vingerhoets, D. T. Yordanov, and M. Záková, Phys. Rev. C **82**, 051302(R) (2010).

[3] A. Gottardo, D. Verney, C. Delafosse, F. Ibrahim, B. Roussière, C. Sotty, S. Roccia, C. Andreoiu, C. Costache, M. C. Delattre, I. Deloncle, A. Etilé, S. Franchoo, C. Gaulard, J. Guillot, M. Lebois, M. MacCormick, N. Marginean, R. Marginean, I. Matea, C. Mihai, I. Mitu, L. Olivier, C. Portail, L. Qi, L. Stan, D. Testov, J. Wilson, and D. T. Yordanov, Phys. Rev. Lett. **116**, 182501 (2016).

[4] T. J. Procter, J. Billowes, M. L. Bissell, K. Blaum, F. C. Charlwood, B. Cheal, K. T. Flanagan, D. H. Forest, S. Fritzsche, C. Geppert, H. Heylen, M. Kowalska, K. Kreim, A. Krieger, J. Krämer, K. M. Lynch, E. Mané, I. D. Moore, R. Neugart, G. Neyens, W. Nörtershäuser, J. Papuga, M. M. Rajabali, H. H. Stroke, P. Vingerhoets, D. T. Yordanov, and M. Záková, Phys. Rev. C **86**, 034329 (2012).

[5] P. Campbell, I. D. Moore, and M. R. Pearson, Prog. Part. Nucl. Phys. **86**, 127 (2016).

[6] K. Sieja and F. Nowacki, Phys. Rev. C **85**, 051301(R) (2012).
[7] Y. Tsunoda, T. Otsuka, N. Shimizu, M. Honma, and Y. Utsuno, Phys. Rev. C **89**, 031301(R) (2014).
[8] G. Hagen, G. R. Jansen, and T. Papenbrock, Phys. Rev. Lett. **117**, 172501 (2016).
[9] F. Nowacki, A. Poves, E. Caurier, and B. Bounthong, Phys. Rev. Lett. **117**, 272501 (2016).
[10] S. Franchoo, M. Huyse, K. Kruglov, Y. Kudryavtsev, W. F. Mueller, R. Raabe, I. Reusen, P. Van Duppen, J. Van Roosbroeck, L. Vermeeren, A. Wöhr, H. Grawe, K.-L. Kratz, B. Pfeiffer, and W. B. Walters, Phys. Rev. C **64**, 054308 (2001).
[11] K. T. Flanagan, P. Vingerhoets, M. Avgoulea, J. Billowes, M. L. Bissell, K. Blaum, B. Cheal, M. De Rydt, V. N. Fedosseev, D. H. Forest, C. Geppert, U. Köster, M. Kowalska, J. Krämer, K. L. Kratz, A. Krieger, E. Mané, B. A. Marsh, T. Materna, L. Mathieu, P. L. Molkanov, R. Neugart, G. Neyens, W. Nörtershäuser, M. D. Seliverstov, O. Serot, M. Schug, M. A. Sjoedin, J. R. Stone, N. J. Stone, H. H. Stroke, G. Tungate, D. T. Yordanov, and Y. M. Volkov, Phys. Rev. Lett. **103**, 142501 (2009).
[12] B. Cheal, E. Mané, J. Billowes, M. L. Bissell, K. Blaum, B. A. Brown, F. C. Charlwood, K. T. Flanagan, D. H. Forest, C. Geppert, M. Honma, A. Jokinen, M. Kowalska, A. Krieger, J. Krämer, I. D. Moore, R. Neugart, G. Neyens, W. Nörtershäuser, M. Schug, H. H. Stroke, P. Vingerhoets, D. T. Yordanov, and M. Záková, Phys. Rev. Lett. **104**, 252502 (2010).
[13] C. J. Prokop, B. P. Crider, S. N. Liddick, A. D. Ayangeakaa, M. P. Carpenter, J. J. Carroll, J. Chen, C. J. Chiara, H. M. David, A. C. Dombos, S. Go, J. Harker, R. V. F. Janssens, N. Larson, T. Lauritsen, R. Lewis, S. J. Quinn, F. Recchia, D. Seweryniak, A. Spyrou, S. Suchyta, W. B. Walters, and S. Zhu, Phys. Rev. C **92**, 061302(R) (2015).
[14] C. Babcock, H. Heylen *et al.*, Phys. Lett. B **750**, 176 (2015).
[15] T. E. Cocolios, A. N. Andreyev, B. Bastin, N. Bree, J. Büscher, J. Elseviers, J. Gentens, M. Huyse, Y. Kudryavtsev, D. Pauwels, T. Sonoda, P. Van den Bergh, and P. Van Duppen, Phys. Rev. Lett. **103**, 102501 (2009).
[16] T. Otsuka, M. Honma, and T. Mizusaki, Phys. Rev. Lett. **81**, 1588 (1998).
[17] P. Vingerhoets, K. T. Flanagan *et al.*, Phys. Lett. B **703**, 34 (2011).
[18] E. Kugler, Hyperfine Interact. **129**, 23 (2000).
[19] A. Herlert, Nucl. Phys. News **20**, 5 (2010).
[20] A. Gottberg *et al.*, Nucl. Instrum. Methods B **336**, 143 (2014).
[21] B. A. Marsh *et al.*, Nucl. Instrum. Methods B **317**, 550 (2013).
[22] H. Frånberg *et al.*, Nucl. Instrum. Methods B **266**, 4502 (2008).
[23] E. Mané *et al.*, Eur. Phys. J. A **42**, 503 (2009).
[24] B. Cheal *et al.*, J. Phys.: Conf. Ser. **381**, 012071 (2012).
[25] N. J. Stone, At. Data Nucl. Data Tables **90**, 75 (2005).
[26] T. E. Cocolios *et al.*, Nucl. Instrum. Methods B **317**, 565 (2013).
[27] K. M. Lynch, J. Billowes, M. L. Bissell, I. Budinčević, T. E. Cocolios, R. P. De Groote, S. De Schepper, V. N. Fedosseev, K. T. Flanagan, S. Franchoo, R. F. Garcia Ruiz, H. Heylen, B. A. Marsh, G. Neyens, T. J. Procter, R. E. Rossel, S. Rothe, I. Strashnov, H. H. Stroke, and K. D. A. Wendt, Phys. Rev. X **4**, 011055 (2014).
[28] T. E. Cocolios, R. P. de Groote *et al.*, Nucl. Instrum. Methods B **376**, 284 (2016).
[29] D. Rapp and W. E. Francis, J. Chem. Phys. **37**, 2631 (1962).
[30] R. P. de Groote, I. Budinčević, J. Billowes, M. L. Bissell, T. E. Cocolios, G. J. Farooq-Smith, V. N. Fedosseev, K. T. Flanagan, S. Franchoo, R. F. Garcia Ruiz, H. Heylen, R. Li, K. M. Lynch, B. A. Marsh, G. Neyens, R. E. Rossel, S. Rothe, H. H. Stroke, K. D. A. Wendt, S. G. Wilkins, and X. Yang, Phys. Rev. Lett. **115**, 132501 (2015).
[31] F. Weinholtz and ISOLTRAP (private communication).
[32] C. Guénaut, G. Audi, D. Beck, K. Blaum, G. Bollen, P. Delahaye, F. Herfurth, A. Kellerbauer, H. J. Kluge, J. Libert, D. Lunney, S. Schwarz, L. Schweikhard, and C. Yazidjian, Phys. Rev. C **75**, 044303 (2007).
[33] B. Cheal and K. T. Flanagan, J. Phys. G: Nucl. Phys. **37**, 113101 (2010).
[34] R. P. de Groote, M. Verlinde, V. Sonnenschein, K. T. Flanagan, I. Moore, and G. Neyens, Phys. Rev. A **95**, 032502 (2017).
[35] U. I. Safronova *et al.*, J. Phys. B: At. Mol. Opt. Phys. **39**, 749 (2006).
[36] J. Gaiser, Ph.D. thesis, Stanford University, Stanford, California, USA, 1982, SLAC-0255 (unpublished).
[37] T. Skwarnicki, Ph.D. thesis, Institute of Nuclear Physics, Cracow, Poland, 1986, DESY-F31-86-02 (unpublished).
[38] N. J. Stone, At. Data Nucl. Data Tables **111**, 1 (2016).
[39] P. Pyykkö, Mol. Phys. **106**, 1965 (2008).
[40] H. H. Stroke, R. J. Blin-Stoyle, and V. Jaccarino, Phys. Rev. **123**, 1326 (1961).
[41] P. Vingerhoets, Ph.D. thesis, KU Leuven, Belgium, 2011 (unpublished).
[42] J. Papuga, Ph.D. thesis, KU Leuven, Belgium, 2015 (unpublished).
[43] L. Weissman, J. Cederkall, J. Äystö, H. Fynbo, L. Fraile, V. Fedosseyev, S. Franchoo, A. Jokinen, U. Köster, G. Martínez-Pinedo, T. Nilsson, M. Oinonen, K. Peräjärvi, M. D. Seliverstov, and ISOLDE Collaboration, Phys. Rev. C **65**, 044321 (2002).
[44] P. Vingerhoets, K. T. Flanagan, M. Avgoulea, J. Billowes, M. L. Bissell, K. Blaum, B. A. Brown, B. Cheal, M. De Rydt, D. H. Forest, C. Geppert, M. Honma, M. Kowalska, J. Krämer, A. Krieger, E. Mané, R. Neugart, G. Neyens, W. Nörtershäuser, T. Otsuka, M. Schug, H. H. Stroke, G. Tungate, and D. T. Yordanov, Phys. Rev. C **82**, 064311 (2010).
[45] M. Wang *et al.*, Chin. Phys. C **36**, 1603 (2012).
[46] I. Dankó, D. Sohler, Z. Dombrádi, S. Brant, V. Krstić, J. Cederkäll, M. Lipoglavšek, M. Palacz, J. Persson, A. Atac, C. Fahlander, H. Grawe, A. Johnson, A. Kerek, W. Klamra, J. Kownacki, A. Likar, L. O. Norlin, J. Nyberg, V. Paar, R. Schubart, D. Seweryniak, D. Vretenar, G. de Angelis, P. Bednarczyk, D. Foltescu, D. Jerrestam, S. Juutinen, E. Mäkelä, B. M. Nyakó, M. de Poli, H. A. Roth, T. Shizuma, Ö. Skeppstedt, G. Sletten, and S. Törmänen, Phys. Rev. C **59**, 1956 (1999).
[47] N. Shimizu, arXiv:1310.5431.
[48] M. Honma, T. Otsuka, B. A. Brown, and T. Mizusaki, Phys. Rev. C **69**, 034335 (2004).
[49] M. Honma, T. Otsuka, T. Mizusaki, and M. Hjorth-Jensen, Phys. Rev. C **80**, 064323 (2009).
[50] J. M. Allmond, B. A. Brown, A. E. Stuchbery, A. Galindo-Uribarri, E. Padilla-Rodal, D. C. Radford, J. C. Batchelder, M. E. Howard, J. F. Liang, B. Manning, R. L. Varner, and C. H. Yu, Phys. Rev. C **90**, 034309 (2014).
[51] A. Ekström, J. Cederkäll, C. Fahlander, M. Hjorth-Jensen, F. Ames, P. A. Butler, T. Davinson, J. Eberth, F. Fincke, A. Görgen, M. Górska, D. Habs, A. M. Hurst, M. Huyse, O. Ivanov, J. Iwanicki, O. Kester, U. Köster, B. A. Marsh, J. Mierzejewski, P. Reiter, H. Scheit, D. Schwalm, S. Siem, G. Sletten, I. Stefanescu,

G. M. Tveten, J. Van de Walle, P. Van Duppen, D. Voulot, N. Warr, D. Weisshaar, F. Wenander, and M. Zielińska, Phys. Rev. Lett. **101**, 012502 (2008).
[52] G. Neyens, Rep. Prog. Phys. **66**, 633 (2003).
[53] A. Coc *et al.*, Nucl. Phys. A **468**, 1 (1987).
[54] I. Budinčević, J. Billowes, M. L. Bissell, T. E. Cocolios, R. P. de Groote, S. De Schepper, V. N. Fedosseev, K. T. Flanagan, S. Franchoo, R. F. Garcia Ruiz, H. Heylen, K. M. Lynch, B. A. Marsh, G. Neyens, T. J. Procter, R. E. Rossel, S. Rothe, I. Strashnov, H. H. Stroke, and K. D. A. Wendt, Phys. Rev. C **90**, 014317 (2014).
[55] D. Zawischa, Phys. Lett. B **155**, 309 (1985).
[56] P. Lievens *et al.*, Europhys. Lett. **33**, 11 (1996).
[57] S. A. Ahmad *et al.*, Nucl. Phys. A **483**, 244 (1988).